POLITECNICO DI TORINO
Repository ISTITUZIONALE

On the Assessment of an Unstructured Finite-Volume DES/LES Solver for Turbomachinery Applications

(Article begins on next page)

04 August 2020

On the Assessment of an Unstructured Finite-Volume DES/LES Solver for Turbomachinery Applications

CHIARA BERNARDINI, MAURO CARNEVALE,
SIMONE SALVADORI, FRANCESCO MARTELLI
Department of Energy Engineering "S. Stecco"
University of Florence
Via S. Marta, 3 - 50139 Florence
ITALY
chiara.bernardini@unifi.it; mauro.carnevale@unifi.it;
simone.salvadori@unifi.it; francesco.martelli@unifi.it

Abstract: - Improvements in mean flow and performances simulation in turbomachinery has brought research to focus more demanding topics like turbulence effects on turbines. Although overall performances are well predicted by Unsteady-RANS, other phenomena such as aerodynamic noise or transition need more accurate prediction of turbulent flow features. Thus different kinds of equation modeling other than URANS are needed to cope with this issue. The success of Detached-Eddy Simulation and Large-Eddy Simulation applications in reproducing physical behavior of flow turbulence is well documented in literature. Despite that, LES simulations are still computationally very expensive and their use for investigating industrial configurations requires a careful assessment of both numerical and closure modeling techniques. Moreover LES solvers are usually developed on a structured mesh topology for sake of simplicity of high-order schemes implementation. Application to complex geometries like those of turbomachinery is therefore difficult. The present work addresses this issue considering the feasibility of converting an operative in-house URANS solver, widely validated for applicative purposes, into higher resolution DES and LES, in order to face turbulence computation of turbomachinery technical cases. The solver presents a 3D unstructured finite-volume formulation, which is kept in LES approach in order to handle complex geometries and it is developed to perform unsteady simulations on turbine stages. Preliminary assessment of the solver has been performed to evaluate and improve the accuracy of the convective fluxes discretization on an inviscid bump test case. First a DES-based approach has been implemented, as it is less computationally challenging and numerically demanding than LES. A square cylinder test case has been assessed and compared with experiments. Then, a pure LES with a Smagorinsky sub-grid scale model has been evaluated on the test case of incompressible periodic channel flow in order to assess the capability of the solver to correctly sustain a time developing turbulent field.

Key-Words: DES, Inflow Boundary, Numerical accuracy, Turbulent channel flow, Unstructured LES

1 Introduction

Current Unsteady Reynolds-Averaged Navier-Stokes (URANS) simulation methodology for turbulent flows is able to reproduce coherent vortical structures while is not adequate when the topic of interest is the physical behavior of small scales. Then, URANS is widely used in turbomachinery flows with the assumption that the obtained results are sufficiently accurate to predict macro-parameters of industrial interest with a relatively limited computational effort.

It must be pointed out that high Reynolds number (Re) flows contain a broad range of length and time scales. The largest length scale is related to the test case geometry and flow boundary conditions whereas it is mainly at smaller scales that the energy

is transferred down to the smallest dissipative scales. As a consequence, sub-grid scale models are necessary to ensure the accurate computation of the largest resolved motions, which are responsible for the primary jet transport and entrainment. Simulations that capture all the relevant length scales of motion providing the numerical solution of the Navier-Stokes Equation (NS) are termed Direct Numerical Simulation (DNS). DNS is prohibitively expensive, now and for the foreseeable future for most practical flows of moderate to high Re. Large Eddy Simulation (LES) is an alternative both to RANS and DNS methods which provides to capture smaller vortical structures up to wave lengths in the inertial sub-range. Moreover, LES has been demonstrated to be both a useful research tool for

understanding the physics of turbulence, and an accurate predictive method for engineering flows engineering [1][2][3][4].

The LES approach is based on a scale separation, the smallest scales of turbulence being modeled by means of a sub-grid scale model. This methodology is based on the local classical hypothesis proposed by Kolmogorov, which states that the smallest scales of the flow have an universal character and are isotropic. Under this hypothesis, only the largest scales of motions could be retained thus reducing the computational cost still capturing the desired features of the flow [5].

RANS methodologies simulating mean flows have given important suggestions to turbine design, but in order to further increase the reached level of performances and noise abatement, unsteady flows must be addressed and investigated more in depth. Deeper insight is needed on turbulent flow features in order to understand the mechanisms bringing to aerodynamic noise generation and losses, which can then indicate possible ways of intervention. LES solvers are usually developed for structured grids with very high order of accuracy, which are nevertheless not very flexible for complex geometries such as those ones present in turbomachinery.

This paper describes the preliminary results of a research program aiming to convert the operative in-house URANS solver HybFlow, widely validated for applicative purpose, into a higher resolution DES and LES code, while retaining the flexibility features which allow handling complex geometries and high Reynolds flows typical of turbomachinery technical cases.

2 Problem Formulation

The rationale of the work is to analyze and improve the performances of a robust implicit unstructured in-house URANS code, validated for the unsteady aero-thermal analysis of turbomachinery flows, to the levels required by LES. The scope of this activity is not in the realization of the nth code that will perform state-of-the-art LES of channel flows or low-Mach number airfoils. The aim is to join the accuracy provided by LES with the flexibility of unstructured meshes to manage with industrial test cases.

Many problems must be solved to accomplish this result. An explicit time-accurate scheme must be implemented and the real accuracy of the code must be initially investigated. Once the sub-grid scale model and the wall treatment will be implemented, the performances of the code must be

investigated considering standard test cases. Special attention must be paid to the definition of the inflow turbulence boundary conditions as well as the treatment of low Mach compressible flows.

Once these points will be overcome, the remaining issues will be dealt with. This paper describes in detail the way the authors decided to manage the solver development with the presented road map.

2.1 HybFlow Numerical features

The compressible NS equations are written in strong conservative form for a perfect gas. The equations deal with either stationary or rotating reference frames thanks to the addition of centrifugal and Coriolis source terms. The solver has been already documented in [6][7][8] and only a brief description will be given here. The spatial discretization is based on an up-wind Total Variation Diminishing (TVD) finite volume scheme developed for hybrid unstructured grids. Roe's approximate method is used for the up-wind scheme [9] and a least-squares linear reconstruction of the solution inside the elements provides a second order accuracy. Monotonicity of the solution is ensured through the TVD concept based on a non-linear slope limiter. The steady solver is based on an iterative implicit time-marching solution. The implicit iterative time-relaxed Newton method is applied along with the linear solver GMRES coupled to an incomplete ILU(0) factorization [10]. The implicit formulation with a dual-time stepping approach is applied to get the convergence to the physical unsteady time level from the implicit steady solver. Implicit residual smoothing can be applied to the internal time-marching iterations of the scheme to improve stability and convergence. This kind of formulation for each time step allows a quite arbitrarily choice of time step, not drawing any constraint on the Courant (CFL) number. A detailed description of the implicit solver can be found in [6]. Turbulence is usually modeled using the classical eddy-viscosity assumption through the two equation k-ω model proposed by Wilcox [11]. The turbulence model also incorporates an extra algebraic equation, which enforces the physical constraint on the turbulent timescale as proposed by Medic and Durbin [12]. The SST model by Menter [13] has also been implemented. Amongst the transition modeling methods, the k-ε-k_l model and the transport of the intermittency function γ have been implemented. In the first method a term of production of laminar kinetic energy is introduced as suggested by Walters and Leylek [14]. The method based on the

intermittency function needs a coupling with the k-ω or the SST model and is based on the estimation of the momentum thickness, followed by the tuning of the transition correlations on local quantities and then on the use of intermittency function γ. The transport equation for the intermittency function has been implemented following the idea of Abu-Ghannan and Shaw [15]. The function written for γ is coupled with a transition onset function that is solved together with the turbulent closure equations. A detailed description of the implementation and validation of the model can be found in the work by Salvadori et al. [16]. Concerning the computational capabilities, the parallel solver balances the computational load of the code partitioning the grid in blocks that are evenly distributed to the CPUs. The communications between processors are managed by the standard MPI message passing libraries.

3 Problem Solution

As already stated, to transform the described solver into a LES code several changes to the numerical scheme must be considered. In this section each of them addressed and the way they are realized is discussed.

3.1 DES-LES implementation

The implementation of DES and LES in the HybFlow code is now described. All the choices performed by the authors are explained and motivated with respect to the target of the activity.

3.1.1 Explicit time-accurate formulation

The explicit formulation has been implemented to allow resolving the NS equations when considering time/space accuracy of small-scale structures of motion. The solution of NS equations in the grid cells is performed using a two-steps discretization, first spatial and secondly temporal. Two temporal schemes with explicit formulation have been implemented in the solver in the present work: the 2-stages predictor-corrector and the 6-stages 4th order Runge-Kutta scheme. The predictor-corrector algorithm for temporal discretization has been implemented following the formulation known as Henn's method [17]. This method ensures an explicit time resolution while requiring only 2 stages for time advancement. Concerning the explicit formulation a higher order temporal formulation by Calvo et al. [18] has been

implemented on HybFlow. This scheme is an extension of low dissipation and dispersion explicit Runge-Kutta schemes (LDDRK), which are usually employed for solvers requiring high accuracy, as for computational aero-acoustics. The modification by Calvo proposes a 4th order 6-stages Runge-Kutta scheme, which attempts to use minimum storage.

3.1.1 Sub-grid filter for LES and DES

In this section the filtered governing equation for compressible Newtonian fluids, characterizing the LES method, and their implementation on the previously existing solver is described. Let us consider an arbitrary function $F(x_i,t)$, the filtered variable is defined as:

$$\overline{F(x_i,t)} = \int_D G(x_i - \xi_i, \Delta) F(\xi_i,t) d\xi_i \qquad (1)$$

In Eq. 1 G is the filter function and Δ is a measure of the filter width and is related to the computational mesh size [5]. The filtered compressible NS equations are:

$$\frac{\partial \overline{\rho}}{\partial t} + \frac{\partial \overline{\rho}\tilde{u}_i}{\partial x_i} = 0 \qquad (2)$$

$$\frac{\partial \overline{\rho}\tilde{u}_i}{\partial t} + \frac{\partial \overline{\rho}\tilde{u}_i\tilde{u}_j}{\partial x_j} = -\frac{\partial \overline{p}}{\partial x_i} + \frac{\partial T_{ij}}{\partial x_j} \qquad (3)$$

$$\frac{\partial \overline{\rho}\tilde{e}}{\partial t} + \frac{\partial}{\partial x_j}(\overline{\rho}\tilde{e} + \overline{p})\tilde{u}_j = \frac{\partial H_j}{\partial x_j} \qquad (4)$$

$$\overline{p} = \overline{\rho}R\tilde{T} \qquad (5)$$

Here, T_{ij} is the total stress tensor, H_j is the energy flux due to heat transfer and work done by the total stress, and $\overline{\rho e}$ is the filtered total energy per unit volume. The total stress is:

$$T_{ij} = \tau_{ij} + \overline{\sigma}_{ij} \qquad (6)$$

In Eq. 6 τ_{ij} is the sub-grid scale stress tensor and $\overline{\sigma}_{ij}$ is the molecular viscous stress. The closure of the system of equations (2) to (5) requires a model for the sub-grid scale stress τ_{ij} and heat flux H_j, and the specification of appropriate initial and boundary conditions for the flow variables. There are two opposite views regarding the sub-grid scale model.

In the first view, the physical model (e.g. Smagorinsky eddy viscosity) for the sub-grid scale stress τ_{ij} is recognized the only responsible for the entire energy transfer from resolved to sub-grid (unresolved) scales. This requires accurate numerical algorithms, which minimize numerical

dissipation. In the second view (e.g. MILES), the numerical algorithm is held solely responsible for entire energy transfer between resolved and sub-grid scales and no explicit sub-grid scale model is employed. In the present approach, the compressible extension of the Smagorinsky sub-grid scale stress model has been adopted due to its simplicity:

$$\tau_{ij} = 2C_R \overline{\rho} \Delta^2 \sqrt{\widetilde{S}_{kl}\widetilde{S}_{kl}} \left(\widetilde{S}_{ij} - \frac{1}{3}\widetilde{S}_{kk}\delta_{ij} \right) - \frac{2}{3}\overline{\rho}k\delta_{ij} \qquad (7)$$

The rate-of-strain tensor is defined:

$$S_{ij} = \frac{1}{2}\left(\frac{\partial \widetilde{u}_i}{\partial x_j} + \frac{\partial \widetilde{u}_j}{\partial x_i} \right) \qquad (8)$$

Moreover there are hybrid methods views that allow for both sub-grid model and numerical dissipation and U-RANS approach (e.g. DES). Amongst non-zonal approach DES is based on the idea of using RANS turbulence equation sensitized to a filter width Δ in the LES region, which creates a plausible SGS model. According to DES model by Strelets [18] which is based on Menter's SST model, the scale defined in the dissipation term of the transport equation of turbulent kinetic energy is replaced by a DES scale. The dissipation term is then defined as follows:

$$\rho\varepsilon = \beta^* \rho k\omega \rightarrow \beta^* \rho k\omega \cdot F_{DES} \qquad (9)$$

With:

$$F_{DES} = \max\left(\frac{L_{k-\omega}}{C_{DES}\Delta}, 1 \right) \qquad (10)$$

where $\Delta = \max(\Delta x, \Delta y, \Delta z)$ is the maximum local grid spacing, β^* is a constant of SST model, $L_t = \frac{\sqrt{k}}{\beta^*\omega}$ is the turbulent length scale and C_{DES} is the calibration constant of the DES formulation. In the DES model the turbulent scale is replaced by the DES one depending on the relation between the grid and the turbulent local scales: $L_{DES} = min(L_t; C_{DES}\cdot\Delta)$. In this way, as the turbulent scales are smaller than the grid dimension, the SST RANS model is turned on. Otherwise, if the grid is small enough, the SGS term is modeled while the larger scales are resolved. Since the SST model is already present in HybFlow, the DES methodology proposed by Strelets as an extension of Menter's model is carried out.

HybFlow numerical features have been kept unaltered for DES calculation. The spatial fluxes discretization is therefore a second order Roe-upwind scheme. TVD-limiting has been removed as it is believed to be too much dissipative for this kind of simulation. The Runge-Kutta Low-Dispersion-Dissipation, 6 steps at 4th order is used as temporal discretization. Boundary conditions are defined by means of total inlet temperature and pressure, and outlet static pressure, which are defined through similitude from experimental settings.

3.1.2 Reconstruction Correction for Low Mach Compressible Flows

Nowadays increasing power and improvements in numerical methods has led to an extensive use of compressible scheme for simulation in which is important to capture relatively low Mach number. The leading order kinetic energy dissipation rate in a finite volume scheme increases as one over the Mach number, consequently a pure compressible solver, like HybFlow, is sensitive to numerical dissipation increase with decreasing Mach number.

A new algorithm for the low Mach number calculation has been implemented as suggested by Thornber *et al.* [17]. For the second order of accuracy in space Monotone Upstream-centred Schemes for Conservation Laws (MUSCL) method employing the van Leer limiter it was shown that the leading order kinetic energy dissipation rate ε^{M5} could be obtained from Taylor expansion of M5 extrapolation:

$$\varepsilon^{M5} = \frac{\Delta x^5}{60} a u_x u_{xxxxx} + H.O.T. \qquad (11)$$

This term is proportional to Δx^5 as expected from the leading or the difference between the left and right quantities in the expansion of the limiting function. The excessive numerical dissipation is overcome by modifying the velocity jump at the cell interface by a function z, where the reconstruct velocities u are now defined by:

$$u_{L,M5} = \frac{u_L + u_R}{2} + z\frac{u_L - u_R}{2}$$

$$u_{R,M5} = \frac{u_L + u_R}{2} + z\frac{u_R - u_L}{2} \qquad (12)$$

Choosing $z = min (Ma_{local}, 1)$ where $Ma_{local} = max (Ma_L , Ma_R)$ the leading order dissipation rate becomes:

$$\varepsilon^{M5+LM} = \frac{\Delta x^5}{60} \min(|u|, a) u_x u_{xxxxx} + H.O.T. \qquad (13)$$

This ensures that the dissipation does not exceed that of the original scheme and reverts to the standard upwind form in supersonic flows.

3.1.3 Generation of Turbulent Inflow Boundary

In turbulent flow field instantaneous $u(t)$ velocity is the result of two contributions, a mean component and a fluctuating one:

$$u(t) = u_{mean} + u' \qquad (14)$$

The generation of an appropriate correlated turbulence fluctuation at the inlet boundary is a crucial issue in LES. Two different approaches have been implemented. The first one isbased on the method presented by Montomoli and Eastwood [21]. The turbulence is obtained by a preprocessing procedure in which a cube of isotropic, homogeneous turbulence is previously generated. The HybFlow solver reads a two dimensional plane through the box and uses a nearest node search to interpolate the synthetic turbulence variables onto the inlet. The turbulence information consists in three fluctuating velocity component. The procedure of generation of velocity profile has been largely discussed in Cant *et al.* [22]. The code reads the inlet static pressure and temperature *P, T* and the local Mach number *Ma*. From *Ma* and *T* the mean velocity is obtained. In order to close the problem, the hypothesis that the static pressure and temperature do not fluctuate at inlet has been assumed. Static pressure and temperature fluctuations are naturally generated after the first cell. The new instantaneous velocity component is obtained as:

$$u = Ma\sqrt{\gamma RT} + u' \qquad (15)$$

where *u'* is obtained from the cuboid and *u* is the instantaneous velocity. By assuming *V* the module of velocity, the new instantaneous *Ma* is obtained as:

$$Ma = V / \sqrt{\gamma RT} \qquad (16)$$

The signal associated to the velocity fluctuation has been statistically analyzed using the mean value of the Fourier transformation of all the signals in every point of the domain and in all directions. As a consequence of this kind of signal the spectral density $|H_{ij}|$ has been calculated. According to Pope [23] every feature of turbulence has been deduced (See Table 2).

The second method used to provide a suitable inlet turbulent field is based on Monte Carlo simulation considering power-spectral density and cross spectral density as targets. According to the method proposed by Kondo and Murakami [24] based on the idea of Hoshiya [25] the velocity fluctuation $u_i(l,t)$ at inlet point in the flow field that satisfied the prescribed power density and cross-spectral density can be expressed using a trigonometric series with Gaussian random coefficient:

$$u_i(l,t) = \sum_{n=1}^{N} \sum_{p=1}^{l} a_{l,p}(\omega_n t) \cos\{\omega_n t + \Phi_{l,p}(\omega_n)\} + \\ + b_{l,p}(\omega_n t) \sin\{\omega_n t + \Phi_{l,p}(\omega_n)\} \quad (17)$$

In Eq. 17 ω_n is the circular frequency of oscillation and Φ is the phase lag. Moreover, $a_{l,p}(\omega_n,t)$ and $b_{l,p}(\omega_n,t)$ are Fourier coefficient, related to the cross-spectral density matrix, and random value calculated by a random Gaussian distribution with standard deviation equal to 1. These coefficients are calculated as follows:

$$a_{l,p}(\omega_n t) = \sqrt{2\Delta\omega_n} |H_{lp}(\omega_n)| \xi_p(\omega_n) \qquad (18)$$

$$b_{l,p}(\omega_n t) = \sqrt{2\Delta\omega_n} |H_{lp}(\omega_n)| \eta_p(\omega_n) \qquad (19)$$

The value of *l,p* in equation 17, equation 18 and equation 19 denotes the two nodal points related to cross-spectral density while $H_{l,p}(\omega_n)$ is calculated from time series of velocity fluctuation at points *l* and *p*. In particular $H_{lp}(\omega_n)$ is a component of the cross-spectral matrix. The independent Gaussian random numbers $\xi_p(\omega_n)$ and $\mu_p(\omega_n)$ are calculated by a Montecarlo simulation with condition of mean value *0* and standard deviation equal to *1*.

The target power spectral densities and cross-correlation are estimated from the longitudinal correlation *f(r)*, lateral correlation *g(r)*, turbulence intensity and turbulence scale measured by Comte-Bellot and Corrsin [26].

This method has been implemented in two different procedures: turbulence can be generated runtime during the simulation, by calculating *u'* for each time step according to [17]. Moreover a single isotropic cube can be generated and it can be used in the interpolating procedure described in the first method.

3.2   Code Assessment and Results

In the next pages the assessment of the implemented methods and the validation of the DES and the LES approaches are described.

3.2.1 DES Assessment

The implemented DES approach has been tested on the well-known test case of unsteady flow past a square cylinder, which refers to experimental data by Lyn et al. [27].
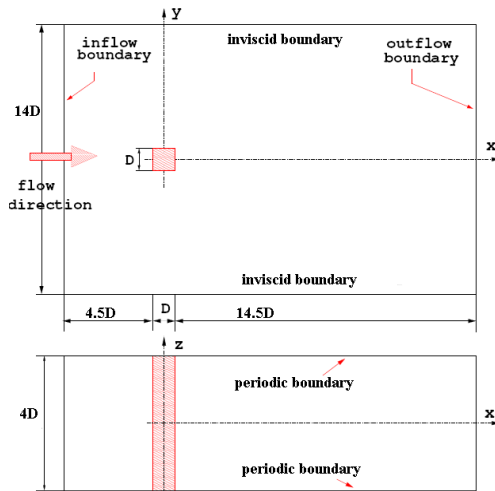

Figure 1 - Square cylinder computational domain

Geometry and computational domain extension are described in Figure 1. The span-wise extension is four times the square side *D*, the inlet boundary is *4.5D* upstream of the cylinder and the outlet *14.5D* downstream the back border of it, which are typical dimensions for a good development of the flow. The hybrid mesh, with 15 prismatic wall layers, is built on the *x-y* plane then extruded in the *z*-direction. In the *x-y* plane the cells are about 58000 and 20 planes are used in *z*-direction, for a total amount of 1.2 millions elements. The first wall node has been positioned at *y/D=0.008* which is a reference value in the literature. The Roe-Upwind method with linear gradient reconstruction has been adopted. As the expected Strouhal number is $St = fD/U=0.13$ corresponding to a shedding frequency of 780 Hz, the chosen time interval yields about 12800 time steps per shedding cycle. Time discretization has been exploited by means of Runge-Kutta method previously presented.

Three shedding periods have been recorded after a transient period. The FFT of lift coefficient of statistically steady solution highlights the frequency of 780Hz, which gives exactly the Strouhal number arising from experiments.

The main aim of this study was to assess the right implementation of the DES model, that is to say the right switch from LES to RANS model. Therefore attention has been paid essentially on this aspect rather than to the turbulence modeling accuracy, which will be analyzed later on in a specifically devoted test case. Vorticity field is fully developed in three dimensions as illustrated by the iso-vorticity magnitude surfaces and the Mach number in the span-wise direction (Figure 2).
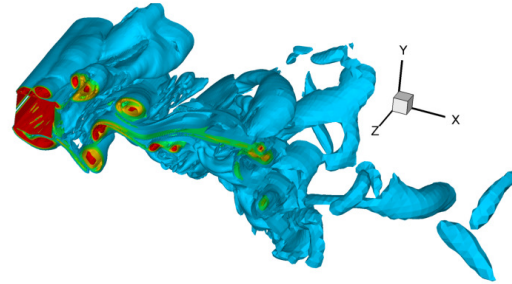

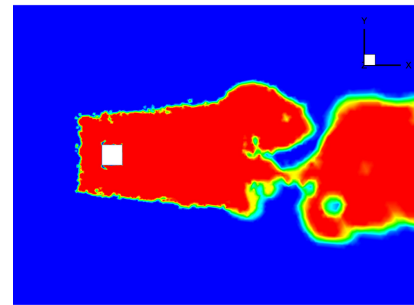**Figure 2 – Instantaneous iso-vorticity surfaces around square cylinder**

Figure 3 – Instantaneous zones of LES (red) and RANS (blue) model in the entire computational domain
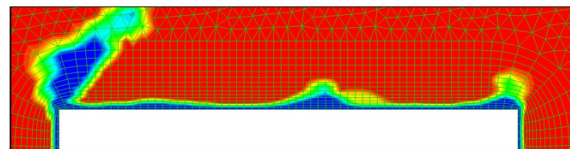

Figure 4 - Instantaneous zones of LES (red) and RANS (blue) model in the wall region

Figure 3 illustrates an instantaneous realization with the zones of the whole domain where the LES model is turned on (red zones) and those using the RANS model (blue ones). The RANS model is exploited in the undisturbed flow. The model switches to LES instead in the zones around the leading edge and at the trailing edge where large-scale vortical structures arises and in the wake region depending on the local turbulent structures length scale. The RANS model turns on in the

proximity of the wall (Figure 4). In this region, as the grid is too coarse and the turbulence length scale is lower than the grid filter (as occurring in the internal boundary layer), the RANS model is activated, the LES model is switched on otherwise. The correct implementation of DES model is then verified, which switches from RANS in the wall region, where the grid is poor for wall turbulence small scales, to LES where the grid is adequately refined for free high turbulence intensity.

The time-averaged x-velocity profiles normal to the wall (Figure 5) exhibit good agreement with experimental data from Lyn et al. in the boundary layer over the cylinder, both in the RANS and LES region, assessing the good ability of the eddy viscosity model to switch from one approach to the other without losing viscous stress information. The agreement is satisfactory also in the recirculating part of the wake, up to *x/D=2.5*. The same behavior is encountered looking at the x-velocity profile along the centerline downstream the cylinder (Figure 6). The discrepancies in the wake region are mainly due to the high numerical dissipation connected to the gradient reconstruction method and to the unstructured grid coarsening in that region. As low numerical dissipation is necessary for the correct performance of LES, the effect of these numerical features is specifically analyzed in the following section.
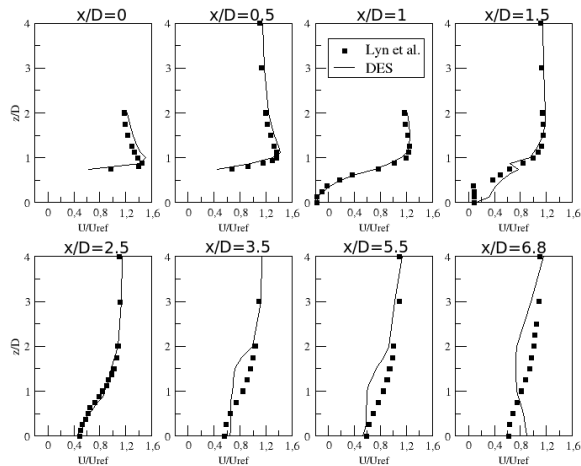

Figure 5 - Time averaged x-velocity profiles normal to the wall - DES on square cylinder
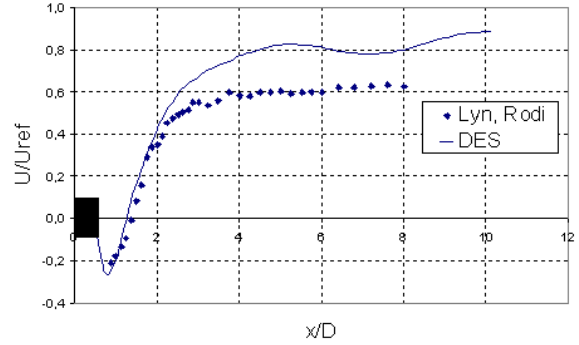

Figure 6 - Time-averaged x-velocity profile along the wake centerline - DES on square cylinder

3.2.2 Analysis of order of accuracy

Since results of DES assessment results have shown a lack in the simulation of the wake region, the accuracy level of HybFlow has been studied to understand if the numerical methodology implemented is sufficient for a LES simulation. The flux numerical discretization has a theoretical order of accuracy which is defined by the numerical scheme used, and is said to be order k if the truncation error is of order $o(x^k)$. The error of the solution should have therefore the same behavior that should be of order k and the solution error should decrease with mesh size according to:

$$\varepsilon \propto h^k \tag{20}$$

where h is the typical mesh size. An analysis of the error has been carried out on structured and unstructured grids to evaluate the influence of a non-uniform mesh on the accuracy. Since the flow is Eulerian the total pressure is supposed to maintain its inlet value, as the flow is isentropic. The numerical discretization error will introduce some dissipation which will result in entropy increase, thus in a total pressure loss. We therefore consider the error in terms of total pressure decrease with respect to isentropic total pressure, named $P_{0\infty}$, which is rendered dimensionless to the value of 1. Each cell i will return its error expressed as $\Delta P_0 = P_{0\infty} - P_{0i}$. The total error ε is then computed as follows:

$$\varepsilon = \sqrt{\sum_1^N \frac{\Omega_i}{\Omega}(P_{0\infty} - P_{0i})^2} \tag{21}$$

where Ω_i is the volume of *i-th* cell and Ω is the total control volume of the geometry. In order to verify the real order of accuracy of the convective term

numerical discretization used in HybFlow, we employ an Eulerian test-case that can underline it by refining the mesh. The 2-dimensional channel in Figure 7 of height L and length 10L has been considered, with a bump put at its center x_0 with height 1/3 of the duct height L. Its profile has been designed in order to preserve the continuity of the second derivative at the beginning point of the bump.
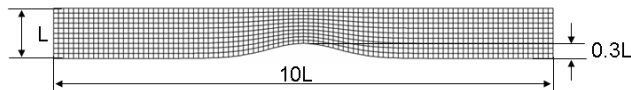

Figure 7 - Geometry of the bump test-case

Boundary conditions have been set in order to avoid choke in the throat. By the area ratio *A/A*=10/7=1.424* the critical Mach number is 0.4, then $p_{out}/p_0 = 0.8956$ is set in order to obtain Mach = 0.4. Meshes have been built to keep the same typical grid size *h*, which represents the height of the structured squared element, and the triangle height in the unstructured grid. This approach brings the unstructured grid to have double number of elements compared to the corresponding structured grid. Grid refinements are shown in Figure 8.
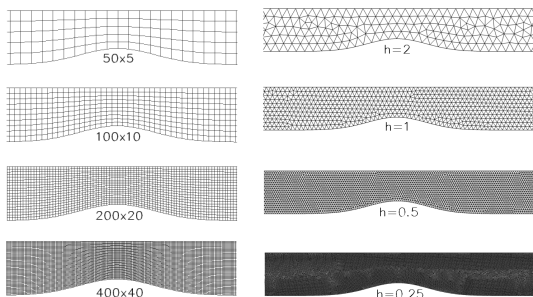

Figure 8 - Bump grid refinement: (left) structured grid and (right) unstructured grid

Both Roe-upwind linear and LSQ gradient reconstruction has been tested on each different mesh size. In Table 1 the test matrix is summarized. For structured grids the results are taken after 150000 iterations, when the residuals were stable at values of the order of 10^{-8}. Figure 9 illustrates the total error ε relative to the mesh size *h* in a logarithmic scale. The resulting error for linear gradient reconstruction has a trend proportional to $h^{1.46}$, that is to say the numerical scheme is not exactly of the second order. We expect a different behavior of the solution coming from the least square reconstruction. In fact the outcome is that the slope of the total error trend with respect to mesh

size *h* is 2.54, higher than the formal second order implemented.

Table 1 - Simulations matrix

Gradient reconstruction	MESH SIZE Struct	MESH SIZE Unstruct
Linear	50x5	h=2
	100x10	h=1
	200x20	h=0.5
	400x40	h=0.25
LSQ	50x5	h=2
	100x10	h=1
	200x20	h=0.5
	400x40	h=0.25

Calculations on the four unstructured grids by means of Roe-Upwind discretization with linear gradient reconstruction have been fulfilled by 150000 iterations with residuals at about 10^{-8}. The error scales as $h^{1.23}$, showing a greater error compared to that of the structured grid, closer to a first than to a second order scheme. Calculations on the unstructured grid with the LSQ gradient reconstruction supply an error scaling as $h^{1.88}$. For the structured grids, the least squares discretization is more accurate than a linear one. Nevertheless, for the structured grids the order of accuracy is still smaller than the expected second order. All results explained above are summarized in Figure 9.
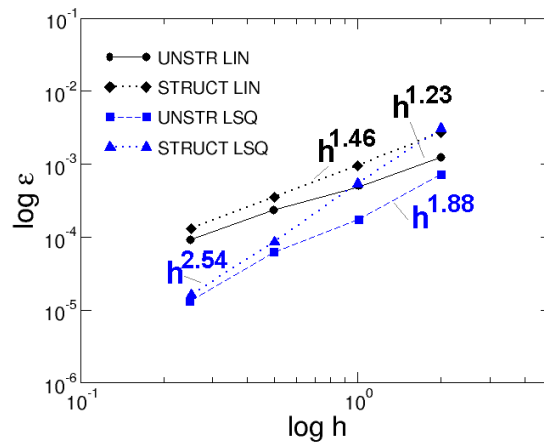

Figure 9 - Numerical schemes errors on structured and unstructured grids

3.2.4 Turbulent channel flow test case

The feasibility of LES methodology on HybFlow solver has been addressed considering the fully develop turbulent channel flow test-case from Kim *et al.* [28] (Figure 10). This would allow stating the capability of the solver to sustain a turbulent field in a closed environment.
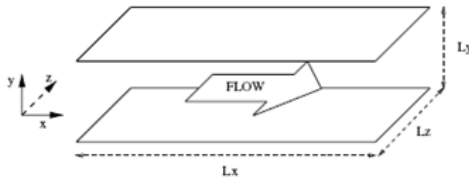
Figure 10 - Channel flow test-case

The flow is characterized by $Re_\tau=180$ and channel's dimensions arise from the study of Jimenez [29] leading to: $L_x= 5/2\pi H$, $L_y=2H$, $L_z=4/3\pi H$ with $H=1$. To represent a fully developed flow, periodic conditions must be applied between inlet and outlet sections. The same periodic condition has been applied in the span-wise direction. Enforcing periodicity in the stream-wise direction requires that the flow must be somehow guided to overcome the resulting pressure drop. The straightforward method adding a forcing term in the x-momentum equation has been first implemented. This external force, which is proportional to the x-direction pressure gradient, is a constant coefficient and is calculated as:

$$f = -\frac{dP}{dx} = -\frac{2\rho_0 u_c^2}{Re_c} = c_f \frac{1}{2}\frac{\rho_0 u_b^2}{H} \quad (22)$$

The assessment of this methodology has been tested on a laminar field in a domain discretized with a structured uniform grid 64x48x48, employing a Roe-Upwind discretization with LSQ reconstruction and explicit time advancement, 2-stage Predictor Corrector, with initialization defined by a parabolic profile with $Ma = 0.1$. This method actually resulted not to be able to preserve the mass-flow thus a new methodology has been implemented.

The algorithm by Lenomard $et\ al$ [30] has been implemented. At each time step the forcing term is updated as follows:

$$f_1^{n+1} = f_1^n + \frac{1}{2HL_z}\Big[\beta_1\big(\dot{M}^{n+1} - \dot{m}\big) + \beta_2\big(\dot{M} - \dot{m}\big)\Big] \quad (23)$$

where $\dot{m} = 2HL_z(\rho u)_b$ is the mass-flow to be preserved based on the desired bulk velocity:

$$\dot{M}^n = L_z \cdot \sum_{i=1}^{N_y} \overline{\rho u}_i dy \quad (24)$$

$$\dot{M}^{n+1} = \dot{M}^n - \Delta t\, 2HL_z f^n + 2L_z\mu\frac{\partial \overline{u}_1}{\partial y}\Big|_{-H} \quad (25)$$

A sensibility analysis led to the optimal choice of the values of $\beta_1=2.0$ and $\beta_2=-0.2$. With this method the mass-flow is preserved after in initial transient and unsteady simulation reproduces exactly the analytical laminar solution as illustrated in Figure 11. The mass-flow is now preserved and equals the enforced value (M set in Figure 11).
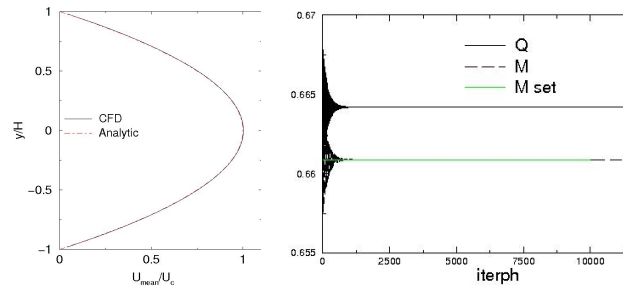

Figure 11 - Mean velocity profile (right); convergence history of volume (Q) and mass-flow (M) rate (left).

After fixing the methodology for correct boundary condition exploitation, the turbulent solution has been addressed in order to verify the capability of the solver to manage LES approach. The fluxes are handled using the discretization that has been demonstrated to supply the highest order that is the Roe-Upwind with LSQ gradient reconstruction. The two-stage predictor-corrector has been adopted as it supplies the same performance in terms of accuracy than the Runge-Kutta (results not shown here).

The Smagorinsky SGS model has been implemented turning off the equation of turbulent kinetic energy and specific dissipation, and implementing the Smagorinsky formulation which links the SGS stress to the SGS turbulent viscosity and averaged field strain rate. The model has been turned on to evaluate the potential of the solver. The Smagorinky constant C_s has been set equal to 0.12.

The initial solution adopted has been interpolated from the results of a DNS calculation of a narrow channel which reproduces a turbulent field with $Re_\tau = 180$. The forcing term is enforced in order to reproduce the desired bulk Reynolds number, which corresponds to a value of the centerline Mach number equal to 0.1. It is indeed very important to recall this while looking at the results, as the solver is asked to reproduce an incompressible field, while its numerical scheme is actually devoted to general compressible flows.

Three grid levels have been considered:
- GRID1 is 64x48x48 (the same level used for the laminar calculation)
- GRID2 is 96x72x72
- GRID3 is 128x96x96.

All grids have a structured uniform pattern as to guarantee the highest available order of accuracy. GRID3 has a first grid node with $y^+\approx1.6$, while the stream-wise and span-wise spacings are respectively $\Delta x^+\approx10$ and $\Delta z^+\approx8$, that are reasonable for a LES on a uniform grid. The time step has been chosen in order to obtain $CFL=1$.

The original reconstruction scheme without the low-Mach number correction has been proven to be too dissipative. This scheme has been adopted on GRID1 and GRID2 without the sub-grid scale dissipative term. Turbulent kinetic energy has been considered at centerline, averaged in span-wise and stream-wise direction (Figure 12). The initial level of k is higher for the fined grid due to the interpolation that retains higher frequency fluctuations than in the coarser grid. As the solution advances in time, fluctuations are damped until they are totally erased.
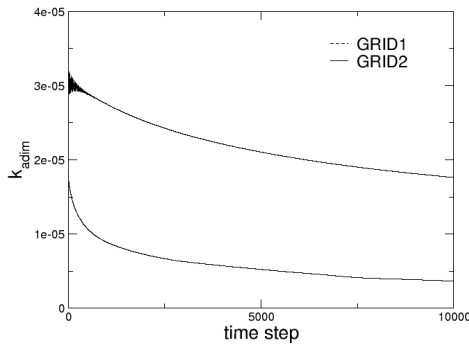

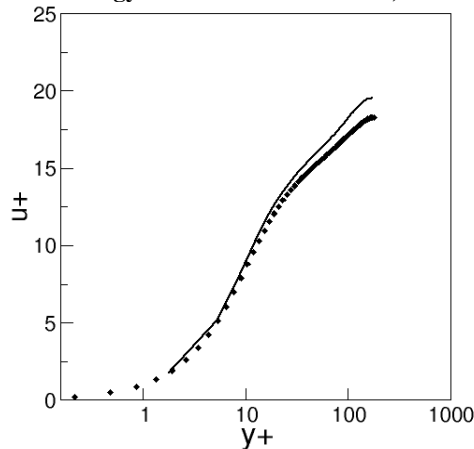Figure 12 - Time history of centreline turbulent kinetic energy for GRID1 and GRID2, no SGS.

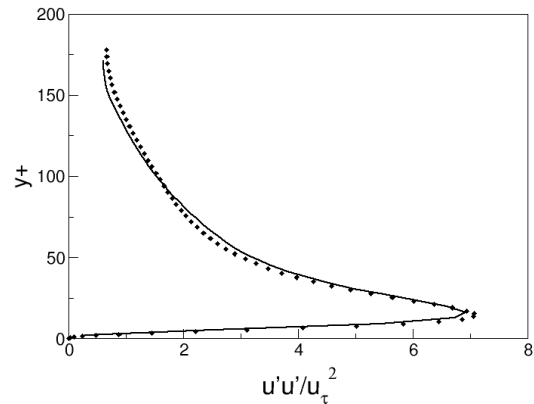Figure 13 - Velocity profile in inner coordinates; LES (bold line) and DNS [28] (diamonds)

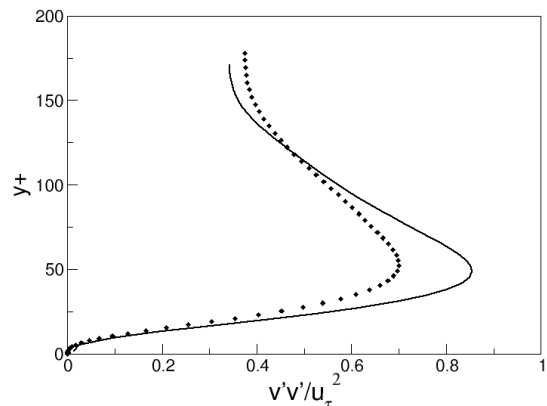Figure 14 – Wall normal distribution of mean normalized resolved u'u' stress; LES (bold line) and DNS [28] (diamonds)

Figure 15 – Wall normal distribution of mean normalized resolved v'v' stress; LES (bold line) and DNS [28] (diamonds)
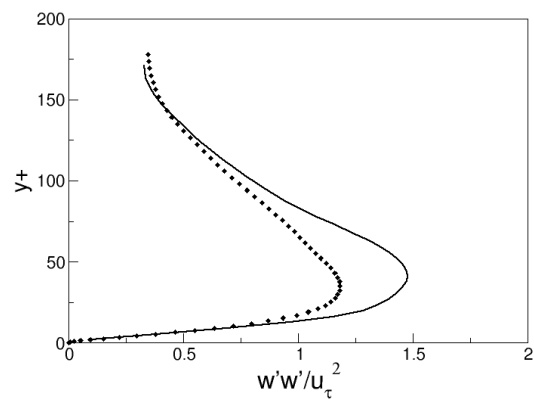

Figure 16 – Wall normal distribution of mean normalized resolved w'w' stress; LES (bold line) and DNS [28] (diamonds)

The excessive dissipation due to the numerical scheme has then been adjusted using the Thornber's correction for low Mach number flows in fluxes reconstruction. The turbulent fluctuations demonstrated to be correctly sustained with this

scheme. After an initial transient the solution reached a statistically steady state. Results have been collected over two eddy turnover time and its statistics is illustrated here, averaged in span-wise and stream-wise direction.

Figure 13 shows the velocity profile in inner coordinates reproducing correctly the viscous sub-layer linear profile. A mild mismatch is noticeable in the inertial sub-layer log-low. This could be accountable to the enforcement of bulk velocity which results in a slight different Re_τ, which assumes the value of 170 instead of 178 as the Kim *et al.* [28] DNS solution. This slight under-prediction is however a consequence of the second-order scheme which may cause this kind of behavior. The stresses are illustrated in Figure 14, Figure 15, Figure 16 rendered dimensionless by the local skin friction velocity and represented in inner-coordinates. There is a very good agreement in the stream-wise fluctuations distribution between DNS and HybFlow LES. The distribution of normal to the wall and span-wise mean-square fluctuations is slightly over-predicted in the peak region at the beginning of the inertial sub-layer at $y^+ \approx 50$, while better agreement can be noticed in the viscous sub-layer.
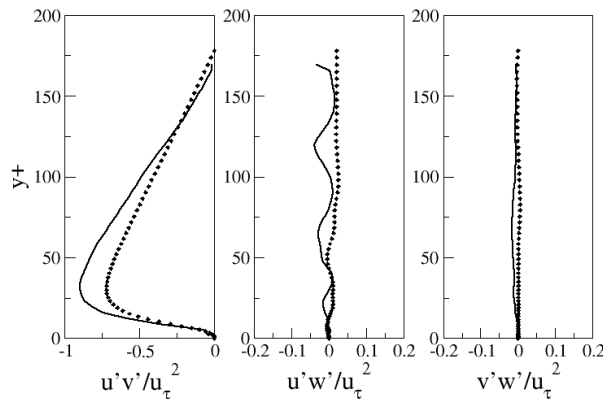

Figure 17 - Distribution of dimensionless resolved $u'_i u'_j$ stresses in inner coordinates
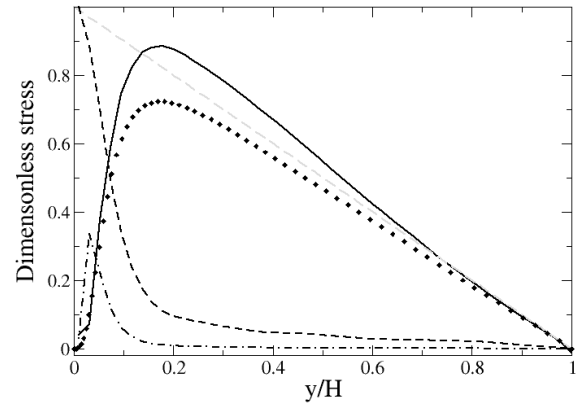

Figure 18 - Normal to wall shear stresses distribution: viscous (dash-dash), resolved turbulent (bold) and sub-grid turbulent stress (dash-dot), compared to experimental turbulent stress (diamonds)

The turbulent shear stresses are illustrated in Figure 17. The order of magnitude and qualitative distribution is correctly reproduced by the LES calculations, although some mismatch is present. These discrepancies can be ascribed to the incompressibility effects on numeric that are stronger close to the wall. The overestimation of the turbulent stresses orthogonal to the flow is also revealed by the profile of the shear stresses in Figure 18. A peak in the unresolved turbulent shear stress (sub-grid shear stress, dash-dot) around *y/H=0.1* confirms the well-known behavior of the Smagorinsky SGS model which needs some kind of wall damping. One of the ongoing developments of the LES solver is actually the implementation of Van Driest damping function, which is intended to fix up this behavior.
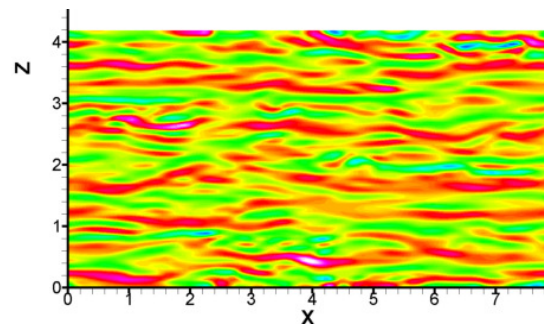

Figure 19 - Instantaneous normal to the wall vorticity component contours in a x-z plane at $y^+ \approx 10$
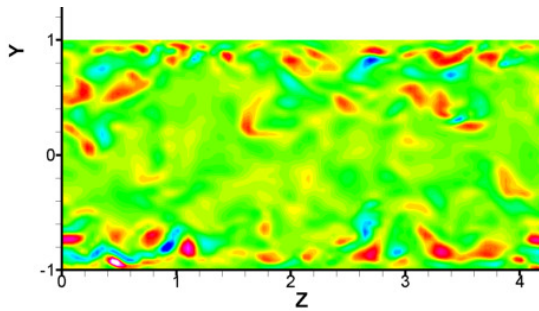
Figure 20 - Instantaneous stream-wise vorticity component contours in a z-y plane at $x/L_x=0.5$

Turbulent fluctuations are sufficiently sustained by the numerical schemes and the typical vortical structures develop inside the channel. Figure 19 illustrates the contours of normal to the wall vorticity component in a plane at $y^+ \approx 10$ which highlights the generation of the typical streamwise streaky structures. This can be possible as the grid spacing is fine enough in the spanwise direction ($\Delta z^+ \approx 8$) to let these wall-layer streaks develop. These structures generates in the viscous sublayer while the "lifted" streaks [29] extend in the buffer layer in a region around $y^+ \approx 30$, as evidenced in the stream-wise vorticity component in a normal to the wall plane at $x/L_x=0.5$ (Figure 20).
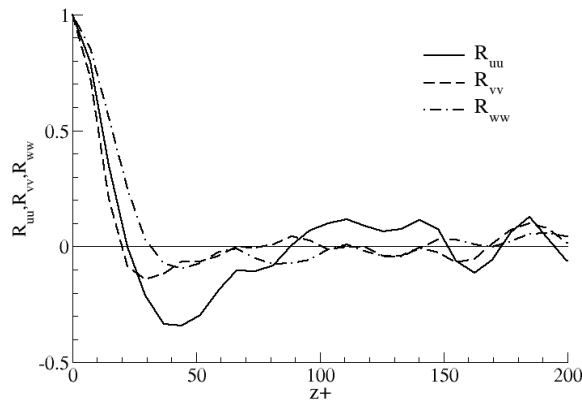

Figure 21 - Spanwise two-point correlations at $y^+ \approx 10$

Quantitative information such as the streaks spacing can be extracted by the two-point correlations of velocity fluctuations in the spanwise direction as illustrated in Figure 21. Their irregular distribution is due to the fact that a single eddy turnover is considered. The autocorrelation of streamwise velocity fluctuations R_{uu} becomes negative and reaches a minimum at $\Delta z^+ \approx 50$ in agreement with DNS data by Kim *et al.* [28]. Following there analysis the mean spacing between the streaks should be twice this distance, so the experimental

value of $\Delta z^+ \approx 100$ is correctly reproduced. The position of the minimum of R_{vv}, which represent the mean diameter of these near wall vortical structures, is slightly overestimated as it is $\Delta z^+ \approx 30$ while in [22] is found to be $\Delta z^+ \approx 25$. The minimum of R_{ww} at $\Delta z^+ \approx 100$ indicate the presence of counter-rotating vortex pairs. The over-prediction of these structures compared to [28] is in accordance with the over-prediction of mean spanwise fluctuations observed in Figure 16.

3.2.5 Turbulence Inflow Boundary Validation

The procedure of producing synthetic turbulence has been set in order to reproduce a cuboid of turbulence with the same statistical characteristic of the test turbulence created and largely discussed in [22]. Table 2 summarizes and compares the principal features for both velocity fluctuations. Referring to Table 2, parameters have been defined as follows:

- $H_{11}(\omega_n)$ is calculated by spectral analysis of autocorrelation signal.
- Turbulence dissipation rate ε_0 can be deduced from the following expression hinging of a prescribed cross spectral matrix

$$H_{11}(k_1) = \frac{18}{55} C_k \varepsilon^{2/3} k_1^{-5/3} \qquad (26)$$

- Taylor microscale can be evaluated as

$$\lambda_0 \approx u'_{rms} \sqrt{15\nu / \varepsilon_0} \qquad (27)$$

- Microscale Reynolds number, is calculated related to Taylor microscale:

$$Re_\lambda = u'_{rms} \lambda_0 / \nu \qquad (28)$$

Where k is the wave number related to the different component of oscillating modes, u'_{rms} is the root mean square of oscillating velocity and ν is the cinematic viscosity.

Table 2 – Features for Test Turbulence and Synthetic Turbulence

	Cant et al.	Bernardini et al.
Urms	0.823	0.898
Vrms	0.818	0.891
Wrms	0.819	0.882
$|H_{ij}|$ (m³/s²)	8.798	9.109
ε_0(m²/s³)	0.420	0.443
Taylor Scale	1.874×10^{-2}	1.991×10^{-2}
Re $_{Taylor}$	1060	1223

Chiara Bernardini, Mauro Carnevale,
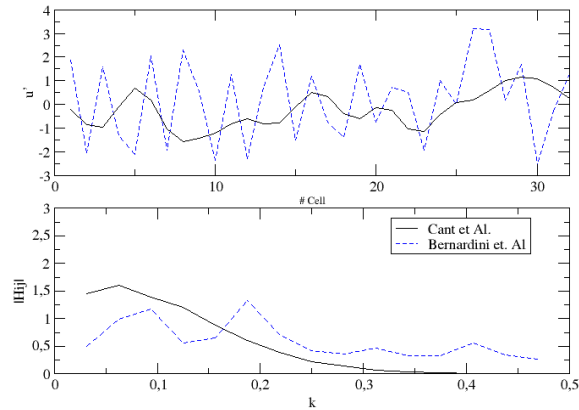Simone Salvadori, Francesco Martelli

Figure 22 – Top: Statistical behaviour of fluctuating energy; Bottom: single signal of u' related to the centre of domain

The behavior of fluctuating velocity is similar both considering the single signal (Figure 22-bottom), both considering the statistical features. In Figure 22-top the mean Fourier Transform of every single signal of fluctuating velocity shows that the contribution in creating turbulence comes from similar value of k. A scaling procedure has been adopted in order to obtain different Taylor transverse microscale, and the different u_{rms}/u_{main} starting from an already existing turbulent isotropic flow. The similarity rescaling has been based on the microscale Reynolds Number and on the ratio u_{rms}/u_{main}. An example of geometrical scaling procedure based on Taylor microscale is shown in Figure 23, in which an initial turbulence (right) characterized by λ is scaled to turbulence with $\lambda/16$.
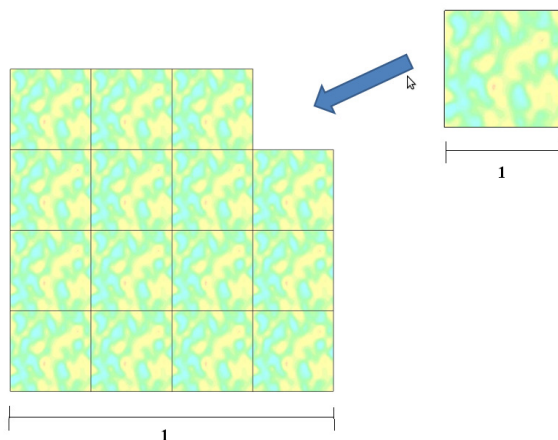

Figure 23 – Geometrical scalature of turbulence.

4 Conclusions

The DES and LES approaches have been implemented and tested in the in-house finite-volume Unsteady RANS solver HybFlow with unstructured grid formulation widely tested for compressible turbine flows.

A preliminary accuracy assessment demonstrated that the convective fluxes gradients reconstruction method affects very much the solver accuracy, which for a formal scheme at the second order brings the effective accuracy from 1.5 to 2.5 with a structured grid. This latter feature is also paramount as with an unstructured grid the effective accuracy becomes lower than two.

The DES approach by Strelets has been implemented which demonstrate the ability of the solver to correctly switch from LES to URANS formulation in the near-wall region.

The capability of HybFlow in sustaining turbulence thus to afford Large-Eddy Simulation has been addressed. The test case adopted is the fully developed turbulent channel flow in a nearly incompressible Mach number range. After having fixed an algorithm for the forcing of the flow with periodic stream-wise conditions, the laminar solution has been tested, which proved a good resolution of the solver. A correction on gradient reconstruction for low-Mach number flows has been adopted in order to prevent excessive numerical dissipation. Turbulence is correctly sustained and the typical near-wall turbulent structures develop. The mean profiles of velocity and turbulent resolved stresses reproduce quite satisfactorily the DNS data, considering the relatively low order of accuracy and the compressible formulation of the solver.

Acknowledgments

References:
[1]   T. Leonard, F. Duchaine, N. Gourdain, L.Y.M. Gicquel, Steady/Unsteady Reynolds Averaged Navier-Stokes and Large Eddy Simulations of a Turbine Blade at High Subsonic Outlet Mach Number, GT2010-22469, 2010.
[2]   N, Gourdain, F. Duchaine; E. Collado; L. Y. M. Gicquel, Advanced Numerical Simulation Dedicated to the Prediction of Heat Transfer in a Highly Loaded Turbine Guide Vane, GT2010-22793, 2010.
[3]   G. Medic, G. Kalitzin, D. You, M. Herrmann, F. Ham, E. Van der Weide, H. Pitsch, J. Alonso, Integrated RANS/LES computations of turbulent flow through a

turbofan jet engine, Center for Turbulence Research Annual Research Briefs 2006.

[4] G. Medic, D. You, G. Kalitzin, An approach for coupling RANS and LES in integrated computations of jet engines, Center for Turbulence Research Annual Research Briefs 2006.

[5] P. Moin and J. Jimenez, Large Eddy simulation of complex Turbulent Flow, AIAA Paper 93-3099, 1993.

[6] P. Adami, F. Martelli, V. Michelassi, Three-Dimensional Investigations for Axial Turbines by an Implicit Unstructured Multi-Block Flow Solver, Proc. ASME IGTI Turbo Expo, Munich, Germany, ASME 2000-GT-0636, 2000.

[7] F. Montomoli, M. Massini, S. Salvadori, Geometrical uncertainty in turbomachinery: Tip gap and fillet radius, Computers and Fluids, 46(1):362-368 (2010)

[8] F. Montomoli, P. Adami, F. Martelli, A finite volume method for the conjugate heat transfer in film cooling devices. In: Proceedings of the institution of mechanical engineers. Part A. J Power Energy 223(A2):191– 200, 2009.

[9] P.L.Roe, Characteristic based scheme for Euler equations, Ann. Rev. Fluid Mech., 1, 1986.

[10] Y. Saad, M.H. Schults, Gmres: a generalized minimal residual algorithm for solving non-symmetric linear systems, SIAM J Sci Stat Comput 7: 856–69, 1986.

[11] D.C. Wilcox, Turbulence Modeling for CFD, DCW Industries Inc., 1993.

[12] G. Medic, P.A. Durbin, 2002, Towards Improved Prediction of Heat Transfer on Turbine Blades, J. Turbomach., 124 (2):187-192, 2002.

[13] F.R. Menter, Improved Two-Equation k-ω Turbulence Models for Aerodynamic Flows. Technical Report, NASA Technical Memorandum 103975, 1992.

[14] D.K. Walters, J.H. Leylek, A New Model for Boundary Layer Transition Using a Single-Point RANS Approach, ASME J. Turbomach., 126(1):193-202, 2004.

[15] B.J. Abu-Ghannam, R. Shaw, Natural Transition of Boundary Layers - The Effects of Turbulence Pressure gradient, and Flow History, Journal Mechanical Engineering Science, 22: 213-228. 1980.

[16] S. Salvadori, C. Bernardini, F. Martelli, P. Adami, Turbulence and transition modeling in transonic turbine stages. In: Proceedings of the ISABE conference; ISABE-2009-1218, 2009.

[17] G. Dahlquist, A. Bjork, Numerical Methods, Englewood Cliffs, NJ: Prentice-Hall, 1974.

[18] M. Calvo, J. M. Franco, and L. Randez. A new minimum storage runge-kutta scheme for computational acoustics. J. Comput. Phys., 201:1-12, 2004.

[19] M. K. Strelets. Detached eddy simulation of massively separated flows. AIAA Paper, 2001-0879, 2001.

[20] B. Thornber, A. Mosedale, D. Drikakis, D. Youngs, R.J.E. Williams, An improverd reconstruction method for compressible flow with low mach number, J. Comp. Ph. 227:4873–4894, 2008.

[21] F. Montomoli, S. Eastwood, Implementation of Synthetic Turbulence Inlet for Turbomachinery LES, *Journal of Computers & Fluids*, 2010.

[22] R.S. Cant, Initial Condition for direct Numerical Simulation of Turbulence, *Cambridge University Internal Report*, 2001.

[23] Pope, S. B, *Turbulenty Flows*, Cambridge University Press, 2000.

[24] K. Kondo, S. Murakami, A. Mochida, Generation of Velocity Fluctuation for Inflow Boundary Condition of LES. *Jounal of Wind Engineering and Industrial Aerodynamincs.* pp 51-64, 1997.

[25] M. Hoshiya, Simulation of multi-correlated random processes and application to structural vibration problems. *Proc. JSCE*, No204 pp 121-128, 1972.

[26] G. Comte-Bellot, S. Corrsin, Simple Eulerian time correlation of full- and narrow-band velocity signals in grid generated, 'isotropic' Turbulence., *Journal of Fluid Mechanics.* Vol. 48, No 2, pp 273-337, 1971.

[27] A. Lyn, S. Einav, W. Rodi, and J.-H. Park. A laser-doppler velocimetry study of ensamble-averaged characteristics of the turbulent near wake of a square cylinder. J. Fluid Mech., 304:285-319, 1995.

[28] J. Kim, P. Moin, and M. Moser. Turbulence statistics in fully developed channel flow at low Reynolds number. J. Fluid Mech., 177:133-166, 1987.

[29] J. Jimenez. The largest scales of turbulent wall flows. Technical report, Center for Turbulence Research Annual Research Briefs, 1998.

[30] E. Lenomard, P. Sagaut, L. Ta Phouc, and P. Compte. Sub-grid scale models for large-eddy simulations of compressible wall bounded flows. AIAA J., 38(8):1340-1350, 2000.